

# Common Envelope Shaping of Planetary Nebulae. IV. From Proto-planetary to Planetary Nebula

Guillermo García-Segura,<sup>1\*</sup> Ronald E. Taam,<sup>2</sup> and Paul M. Ricker<sup>3</sup>

<sup>1</sup>*Instituto de Astronomía, Universidad Nacional Autónoma de México, Km. 107 Carr. Tijuana-Ensenada, 22860, Ensenada, B. C., Mexico*

<sup>2</sup>*Center for Interdisciplinary Exploration and Research in Astrophysics (CIERA), Department of Physics and Astronomy, Northwestern University, 2145 Sheridan Road, Evanston, IL 60208, USA*

<sup>3</sup>*Department of Astronomy, University of Illinois, 1002 W. Green St., Urbana, IL 61801, USA*

Accepted XXX. Received YYY; in original form ZZZ

## ABSTRACT

We present 2D hydrodynamical simulations of the transition of a proto-planetary nebula to a planetary nebula for central stars in binary systems that have undergone a common envelope event. After 1,000 yr of magnetically driven dynamics (proto-planetary nebula phase), a line-driven stellar wind is introduced into the computational domain and the expansion of the nebula is simulated for another 10,000 yr, including the effects of stellar photoionization. In this study we consider central stars with main sequence (final) masses of 1 (0.569) and 2.5 (0.677)  $M_{\odot}$ , together with a 0.6  $M_{\odot}$  main sequence companion. Extremely bipolar, narrow-waisted proto-planetary nebulae result in bipolar planetary nebulae, while the rest of the shapes mainly evolve into elliptical planetary nebulae. The initial magnetic field’s effects on the collimated structures, such as jets, tend to disappear in most of the cases, leaving behind the remnants of those features in only a few cases. Equatorial zones fragmented mainly by photoionization (1  $M_{\odot}$  progenitors), result in “necklace” structures made of cometary clumps aligned with the radiation field. On the other hand, fragmentation by photoionization and shocked wind (2.5  $M_{\odot}$  progenitors) give rise to the formation of multiple clumps in the latitudinal direction, which remain within the lobes, close to the center, which are immersed and surrounded by hot shocked gas, not necessarily aligned with the radiation field. These results reveal that the fragmentation process has a dependence on the stellar mass progenitor. This fragmentation is made possible by the distribution of gas in the previous post-common envelope proto-planetary nebula as sculpted by the action of the jets.

**Key words:** Stars: Evolution – Stars: Rotation – Stars: AGB and post-AGB – Stars: binaries – ISM: planetary nebulae – ISM: individual (Hubble 5, NGC 6302, NGC 2440)

## 1 INTRODUCTION

Planetary Nebulae (PNe) are the final, colorful results of the evolution of low and intermediate mass stars, allowing these stars to become white dwarfs (Kwitter 2022 and references therein). Classical stellar evolution theory combined with hydrodynamical studies (Mellema 1993) explained the formation of PNe in first approximation, but they could not explain the number of high-density structures in PNe (Gonçalves 2001, Mizalski et al. 2009), the existence of collimated structures in proto-planetary nebulae (PPNe; Sahai & Trauger 1998), or the fact that PPNe are characterized by a greater kinetic energy than can be provided by radiation pressure (Bujarrabal et al 2001). In other words, classical stellar evolution theory could not explain the majority of PPNe. However, the binary scenario in general (Soker 1997, De Marco 2009, Jones & Boffin 2017) as well as common envelope evolution (CEE; Paczyński 1971, Taam et al. 1978, De Marco

2009, Ivanova et al. 2013, García-Segura et al. 2018 (paper I), Frank et al. 2018, García-Segura et al. 2020 (paper II), Zou et al. 2020, García-Segura et al. 2021 (paper III), Ondratschek et al. 2022) has been able to provide a consistent explanation for most of the above issues in recent years (De Marco 2009, Blackman 2022).

Binaries and CEE have been invoked to form bipolar PNe in many previous studies, including the references above, but they have not been necessarily involved in the explanation of the formation of elliptical nebulae. Theoretically, models for the formation of elliptical nebulae used ad hoc equations in the past for the asymptotic giant branch (AGB) wind distribution (Icke et al 1989, Mellema et al. 1991, Frank & Mellema 1994) or equations based on the AGB stellar rotation (García-Segura et al. 1999). In this article we show that elliptical nebulae are also a natural consequence of CEE.

Our previous articles (Paper II and Paper III), based on the CEE computations by Ricker & Taam (2012), explored the idea that the gas that remains gravitationally bound after a CEE event is able to form a magnetized, accretion circumbi-

\* E-mail: ggs@astrosen.unam.mx (GGS)

**Table 1.** Initial models from Paper III

Model	$\text{Log } \dot{M}_{\text{AGB}} (\text{M}_{\odot} \text{ yr}^{-1})$	$B_{\phi}$
Fast wind launching		
B6, B7, B8, B9	-6, -7, -8, -9	$1/r$
C6, C7, C8, C9	-6, -7, -8, -9	$1/r^2$
Slow wind launching		
E6, E7, E8, E9	-6, -7, -8, -9	$1/r$
F6, F7, F8, F9	-6, -7, -8, -9	$1/r^2$

nary disk that launches a magnetized wind and jet that can form PPNe with large kinetic energies, consistent with the kinematic analysis of the observations of molecular CO gas (Bujarrabal et al. 2001). In this article, we continue those calculations by incorporating a classic, line-driven, stellar wind as well as the effect of photoionization, to compute the further evolution of the PN phase.

This article is a continuation of Paper III and is structured as follows. The numerical scheme and physical assumptions are described in § 2. The results of the numerical simulations are presented in § 3. Finally, we discuss the numerical results in § 4 and provide the main conclusions in the last section.

## 2 NUMERICAL METHODS AND PHYSICAL ASSUMPTIONS

The numerical simulations have been performed using the magneto-hydrodynamic code ZEUS-3D (Version 3.4), developed by M. L. Norman and the Laboratory for Computational Astrophysics. It is a finite-difference, fully explicit, Eulerian code descended from the code described in Stone & Norman (1992) and in Clarke (1996). A simple approximation is used to derive the location of the ionization front in this study (García-Segura & Franco 1996), assuming that ionization equilibrium applies at all times. The models include the Raymond & Smith (1977) cooling curve above  $10^4$  K. For temperatures below  $10^4$  K, the cooling curve given by MacDonald & Bailey (1981) is applied.

We assume axisymmetry. The 2-dimensional computational grid is in spherical coordinates and consists of  $800 \times 200$  equidistant zones in  $r$  and  $\theta$  respectively, with an angular extent of  $90^\circ$ , and initial radial extent in line with the models of Paper III (see below). A self-expanding grid technique has been employed in order to allow the spatial coordinates to grow by several orders of magnitude.

The injection of mass and momentum into the computational grid representing the stellar wind is treated as an inner boundary condition, covering the two innermost radial zones, and is taken from Villaver et al. (2002), based on the stellar evolution models for zero-age main sequence (ZAMS) masses  $1 M_{\odot}$  and  $2.5 M_{\odot}$  from Vassiliadis & Wood (1994).

For the outer, expanding boundary, we use mass-loss rates between  $10^{-6}$  to  $10^{-9} M_{\odot} \text{ yr}^{-1}$  similar to Paper III. External to the AGB wind, the interstellar medium density is set to  $0.01 \text{ cm}^{-3}$ , which corresponds to densities external to the Galactic spiral arms (Villaver et al. 2012). The AGB wind velocity is assumed to be  $10 \text{ km s}^{-1}$ .

As input for the starting conditions we adopt the computed PPN models from Paper III, displayed in Figure 1 and listed

in Table 1. The snapshots in Figure 1 are taken at 1,000 years from the start of the CEE event for the case of models B and C, and 350 years for models E and F. As a brief summary, Papers II and III explored the further evolution of the ejected envelope computed in a CEE event by Ricker & Taam (2012), the formation of a circumbinary disk by the gravitationally bound gas, the magnetic launching of winds or jets by the circumbinary disk and the formation of PPNe by those computed jets. The computed PPNe were allowed to evolve for a total of 1,000 years, and these are the ones that we use here as initial conditions. In this article we now assume that the central star has reached a  $T_{\text{eff}}=10,000$  K, and photoionization starts to play a role. This properly defines the beginning of a PN, and we set our clock to time=0 in the rest of the article. At the same  $T_{\text{eff}}=10,000$  K, the central star now has a line-driven wind, which we inject in the previously computed PPNe. Models B and C were obtained by a fast, magnetized wind launched from a circumbinary disk in which the binary had an orbital period of 2 days, while models E and F correspond to a slow, magnetized wind that was launched from a binary with an orbital period of 5 days.

The difference between models B and C, and between models E and F, was the treatment of the toroidal magnetic field at the expanding, inner boundary. Models B and E assumed that the field decays as  $1/r$ , while models C and F assumed a  $1/r^2$  behaviour.

During the remainder of this article, we will label the models according to Table 1 for their input model and the mass of the central star; for example, models B6-2.5 and B7-2.5, or models B6-1.0 and B7-1.0.

## 3 RESULTS

For this study we have run a total of 32 numerical simulations for a period of 10,000 years, which is a large fraction of the typical age of the observed PNe (González-Santamaría et al. 2021).

The first 16 computations assume a central, evolving star of  $0.677 M_{\odot}$ , which corresponds to a post-AGB star with a initial mass at ZAMS of  $2.5 M_{\odot}$ . This set of numerical simulations represents an average of PNe progenitors with intermediate mass (between 2 and  $3.5 M_{\odot}$ ). High-mass progenitors would be above  $3.5 M_{\odot}$ .

The other 16 models assume a central post-AGB star of  $0.569 M_{\odot}$ , which descends from a star of  $1.0 M_{\odot}$  at ZAMS. This last set represents the low-mass progenitor population of PNe (below  $2 M_{\odot}$ ).

In all cases, the companion is a  $0.6 M_{\odot}$  main sequence star with neither a stellar wind nor ionizing photons.

The initial conditions for each simulation are taken from Paper III and are used for both sets of models, assuming that the PPN phase, in which the magnetized wind is launched from the circumbinary disk, is similar for all of them, independently of the progenitor mass.

In the next subsections, the results for both stellar models will be displayed in several figures where the density scale bar is different in each panel, with each plot scaled to its minimum and maximum values. Although this could be rather confusing for the reader, it is necessary because the maximum gives valuable information regarding the densities of the clumps that are observed in each model, especially be-

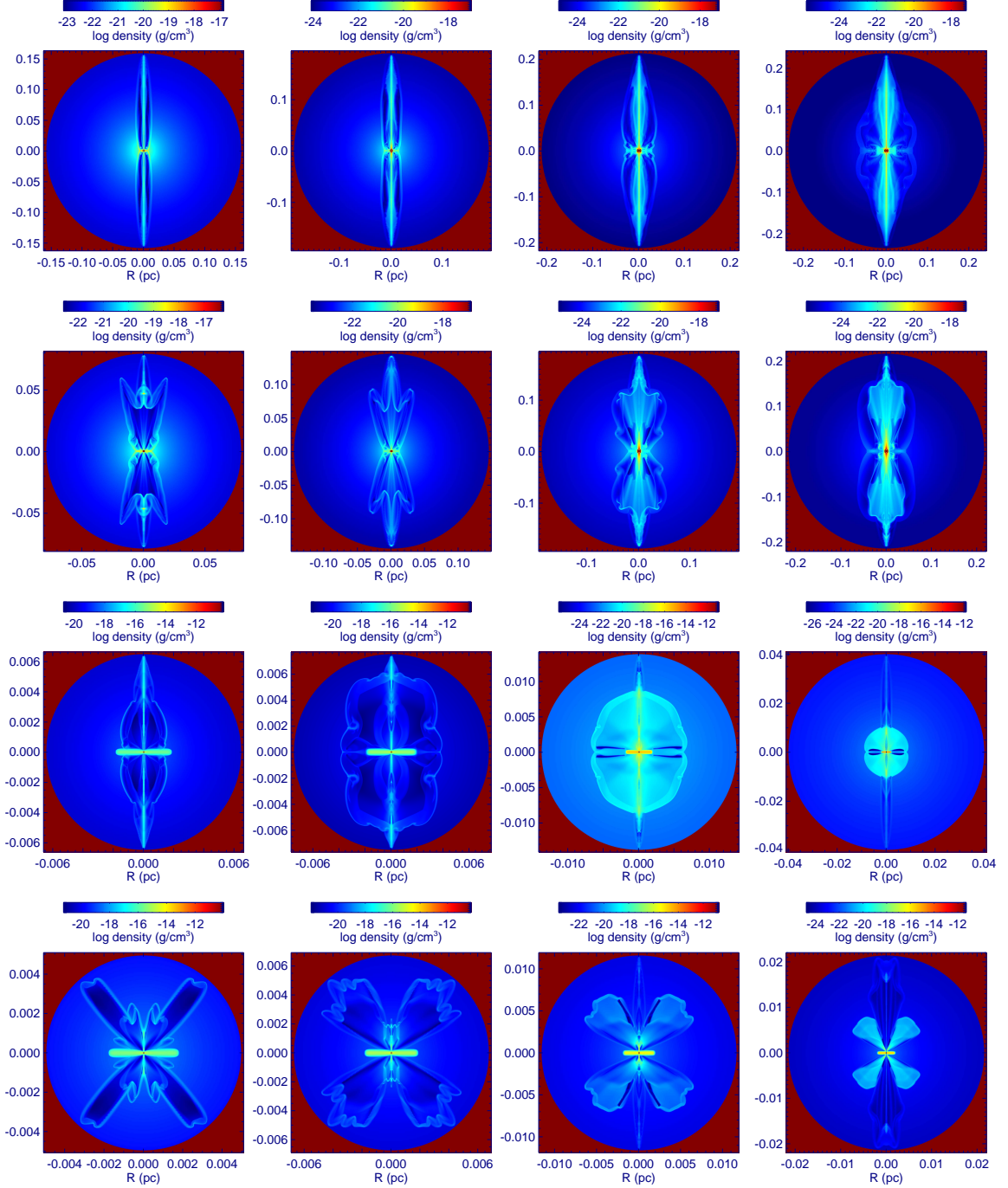


**Figure 1.** Logarithm of density for PPN models B, C, E, F (top to bottom) as shown in Paper III, with logarithm of AGB mass-loss rates in  $M_{\odot} \text{ yr}^{-1}$  of -6, -7, -8, -9 (from left to right). The order is the same as in Table 1.

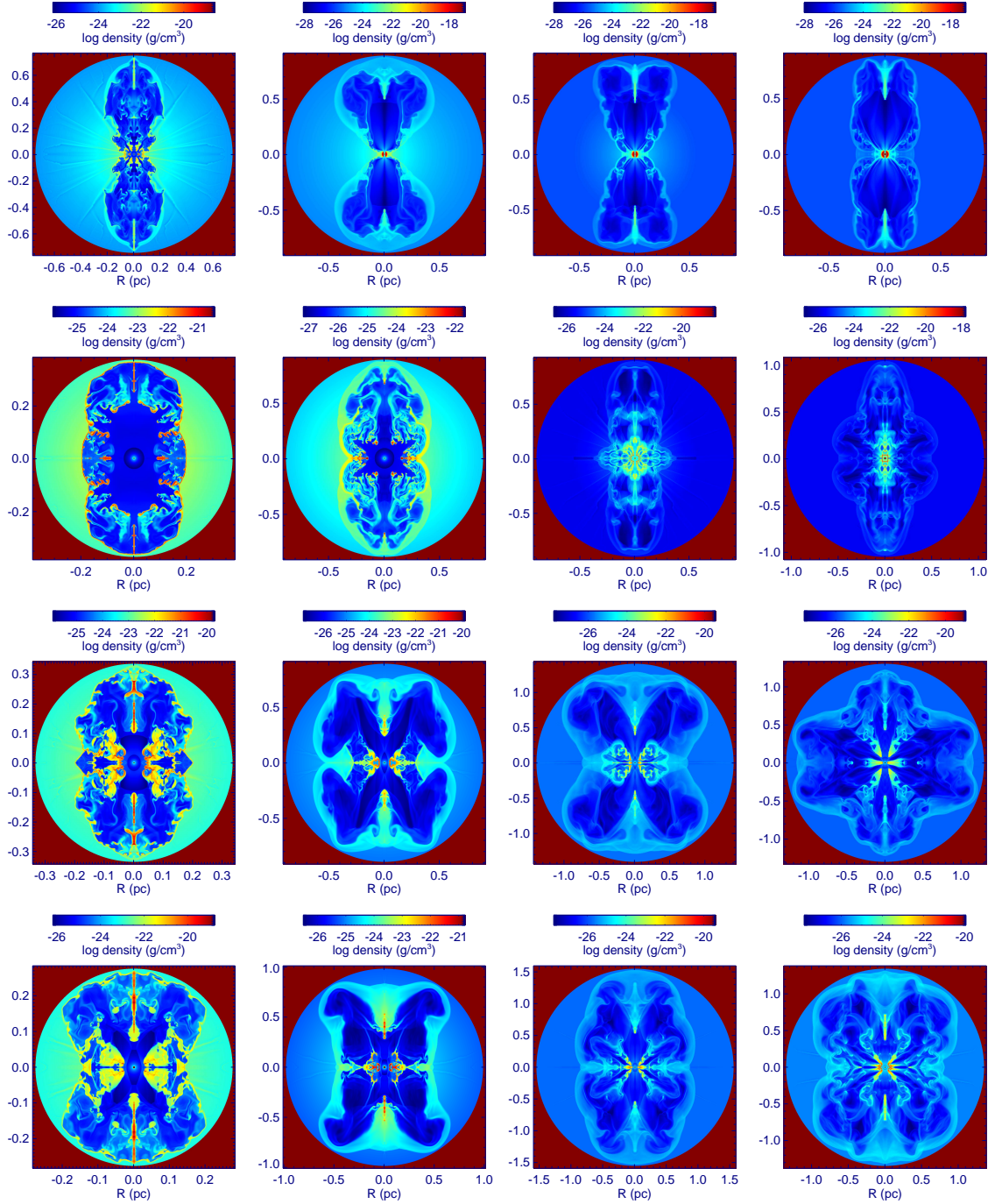


**Figure 2.** Logarithm of density for PN models B, C, E, F (top to bottom), with logarithm of AGB mass-loss rates in  $M_{\odot} \text{yr}^{-1}$  of -6, -7, -8, -9 (from left to right) and a  $2.5 M_{\odot}$  (ZAMS) central star, after 3,000 yr of evolution. The order is the same as in Table 1.

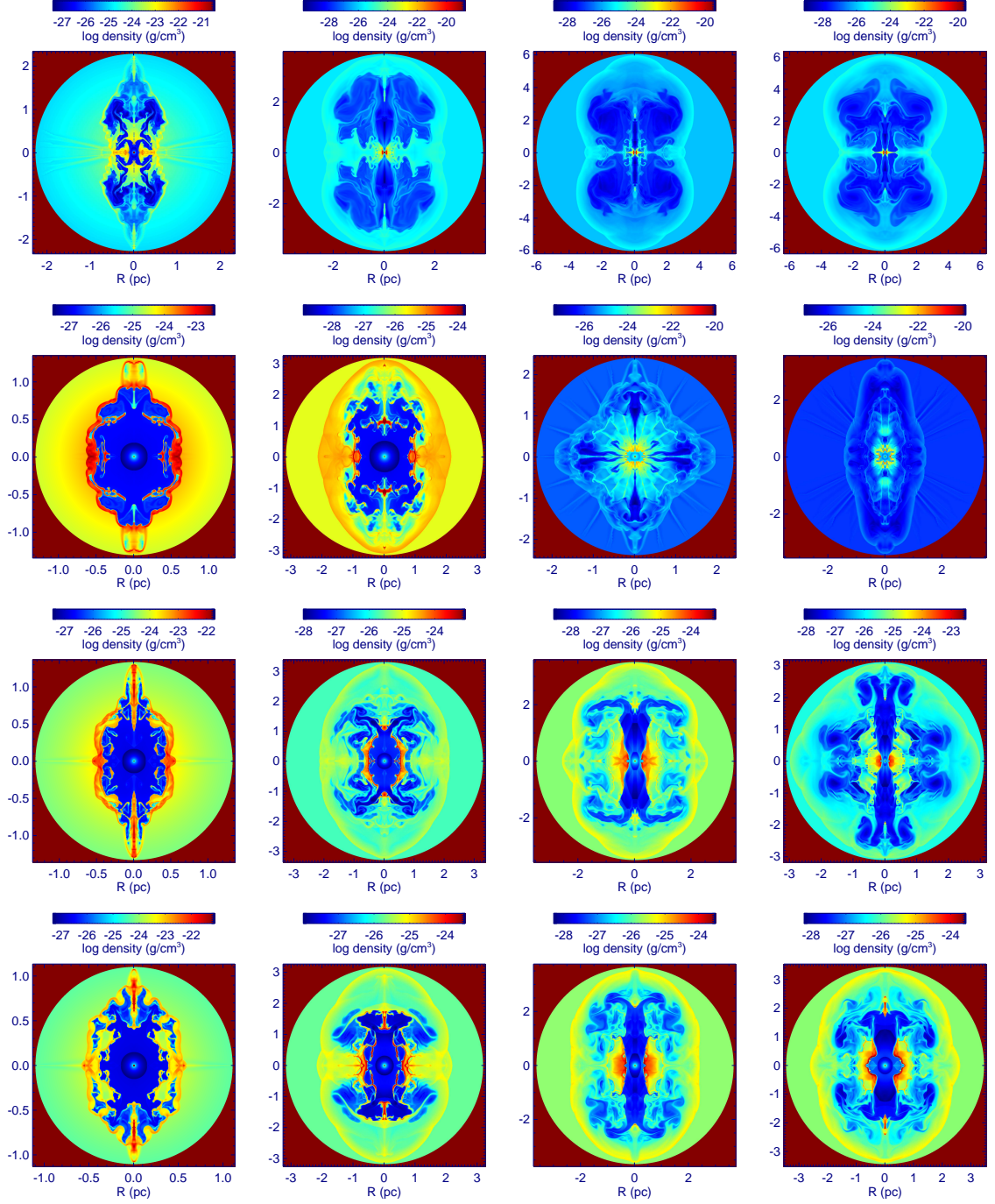


**Figure 3.** Logarithm of density for PN models B, C, E, F (top to bottom), with logarithm of AGB mass-loss rates in  $M_{\odot} \text{ yr}^{-1}$  of -6, -7, -8, -9 (from left to right) and a  $2.5 M_{\odot}$  (ZAMS) central star, after 10,000 yr of evolution. The order is the same as in Table 1.

cause those clumps usually are neutral and are a guide to the densities expected for future H<sub>2</sub> observations, as the James Webb Space Telescope has just shown (De Marco et al. 2022, in preparation).

### 3.1 Results for the 2.5 M<sub>⊙</sub> stellar model

The first 16 computations are shown in Figure 2 at 3,000 yr and Figure 3 at 10,000 yr. To understand the evolution of the computed shapes it is necessary to review first the evolution of the central star.

The figures 3 and 4 in Villaver et al. (2002) show the evolution of the stellar wind kinetic energy and the ionizing photons respectively. For the case of 2.5 M<sub>⊙</sub>, the wind becomes evident at 600 yr after the star reaches T<sub>eff</sub> = 10,000 K, reaching a maximum in its kinetic energy at 2,500 yr. Subsequently, the wind’s momentum and kinetic energy rapidly decline. On the other hand, the number of ionizing photons reaches its maximum at 1,000 yr with a fast decline at 3,000 yr. This is because the blueward evolution of the central star in the HR diagram is fast. As a consequence of the rapid evolution, the wind and the ionizing photons drive the dynamics of the nebula simultaneously.

The snapshots in Figure 2 (3,000 yr) show the computed nebulae at a time near the the peak of their wind kinetic energy, so the action of the winds has been prominent in forming large lobes. For example, models B6-2.5 to B9-2.5 on the upper row of Figure 2, which started as “narrow jet” type PPNe (extremely bipolar) in Figure 1, evolve into narrow waist bipolar PNe, and later into bipolar PNe with large lobes in Figure 3 (10,000 yr). Models C6-2.5 and C7-2.5 have a short bipolar phase (Figure 2) and result in elliptical PNe (Figure 3).

The shape of the outer or forward shock dictates the description of the nebula. In particular, most of the nebulae end up as elliptical nebulae in Figure 3, except for models B (first row in Figures 1 to 3). However, the bright and dense central parts, as in the case of model F8-2.5, can be confused with a bipolar shape.

All models are optically thick to the ionizing radiation at the early phases, and the transition to the optically thin regime occurs as soon as the radiation increases (Figure 4 in Villaver et al. 2002). On the other hand, the transition from an optically thin to optically thick regime occurs when the ionizing radiation declines during the evolution along the white dwarf cooling track. The appearance of spiky features in the density snapshots is a consequence of the optically thick clumps in which the ionization front is trapped locally. The shadows behind the clumps are cold, neutral, and of lower thermal pressure, producing an accumulation of gas from the surrounding photoionized region.

It is also evident that fragmentation can occur either by photoionization or by the hot shocked gas. The process giving rise to the fragmentation will be described in more detail in the discussion section.

### 3.2 Results for the 1.0 M<sub>⊙</sub> stellar model

The second set of 16 computations is shown in Figures 4 (3,000 yr) and 5 (10,000 yr). It is also important to review the history of the wind from the central star for this case.

The history of the wind kinetic energy plotted in figure 3 of Villaver et al. (2002) shows that the wind starts to become dynamically dominant at 10,000 yr (just at the end of our computations), reaching a maximum at 28,000 yr. On the other hand, the number of ionizing photons increases during the total time of our computation (figure 4 of Villaver et al. 2002), and reaches a maximum at 20,000 yr (not seen in their figure 4). According to this scenario, the nebular dynamics are initially driven mainly by the expansion of the H II region, while the action of the wind becomes important later on. For these reasons, the hot shocked gas regions have very small volumes at 3,000 yr (Figure 4), while they begin to be dominant at 10,000 yr (Figure 5).

As in the computations for the 2.5M<sub>⊙</sub> star, we found that the PPNe evolve into bipolar and elliptical PNe. However, the bipolar nebulae have a different structure since they do not form large lobes, but instead are closer in shapes to the original PPNe, with a very narrow waist and very elongated morphology. Their polar expansion velocity is also smaller, by up to a factor of 3. The elliptical shapes in Figure 5 are also more similar to the ones observed in different morphological catalogues (Schwarz, Corradi & Melnick 1992; Machado et al. 1996).

Figures 4 and 5 reveal that some remnants of the PPN jets still survive, specifically for the case of models B6-1.0 to B9-1.0.

Particularly interesting is the equatorial fragmentation of models E-1.0 and F-1.0 in Figure 4, producing a large number of cometary clumps. These might appear as “necklace” structures if one could resolve them in the  $\phi$  direction in 3 dimensions. Although they in principle could form equatorial rings, the ionization front is very efficient in fragmenting the gas into individual clumps, since density fluctuations occurs in all spatial directions (García-Segura et al. 2006).

The cometary clumps (dark red in Figure 4) are neutral and have a bright photoionized head in front. This fragmentation is only produced by the photoionization since the stellar winds are still very weak at 3,000 yr. This is a very interesting result, since the possibility exists to distinguish between models with and without powerful winds, allowing us to infer the mass of the central star.

## 4 DISCUSSION

The primary goal of this paper is to compute the type of ionized nebula resulting from a PPN that has undergone an active magnetic phase after a CEE event. Note that this magnetic activity, produced by a circumbinary disk, is the result of a partial envelope ejection during the CE phase. In the hypothetical case that the envelope ejection is totally successful, the present results are inapplicable since a circumbinary disk will never form. In that case, the structure of the final PN should be similar to those models computed in Paper I.

It should be pointed out that the degree to which the envelope is ejected during the CE phase has not been determined, although Ondratschek et al. (2022) and González-Bolívar et al. (2022) have recently reported that total ejection is possible for a system with an AGB star where the recombination energy of hydrogen and helium can be tapped efficiently. In the case for a low efficiency of the ejection process, on the other hand, a massive circumbinary disk could form; how-

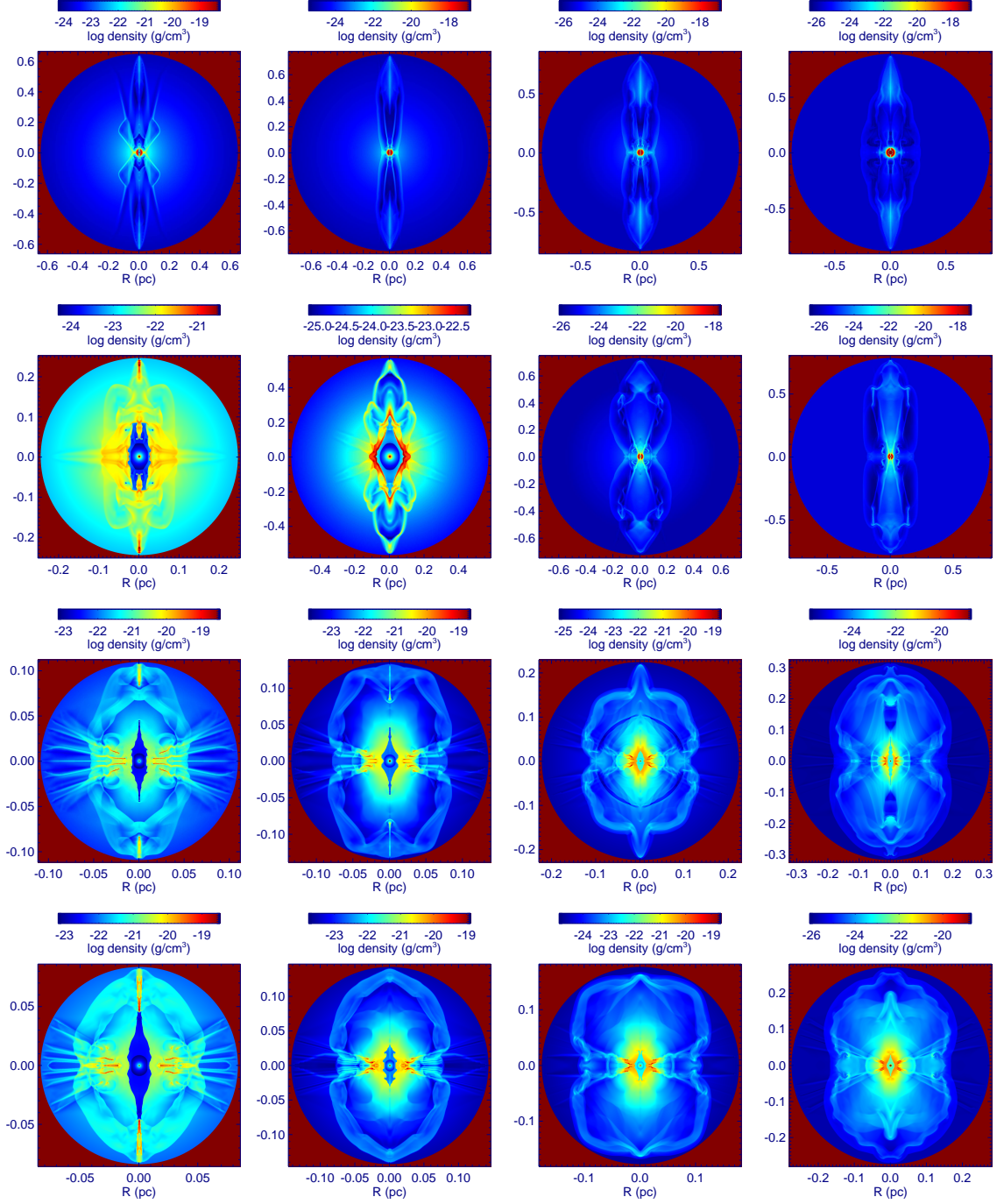


**Figure 4.** Logarithm of density for PN models B, C, E, F (top to bottom), with logarithm of AGB mass-loss rates in  $M_{\odot} \text{yr}^{-1}$  of -6, -7, -8, -9 (from left to right) and a  $1.0 M_{\odot}$  (ZAMS) central star, at 3,000 yr of the evolution. The order is the same as in Table 1.

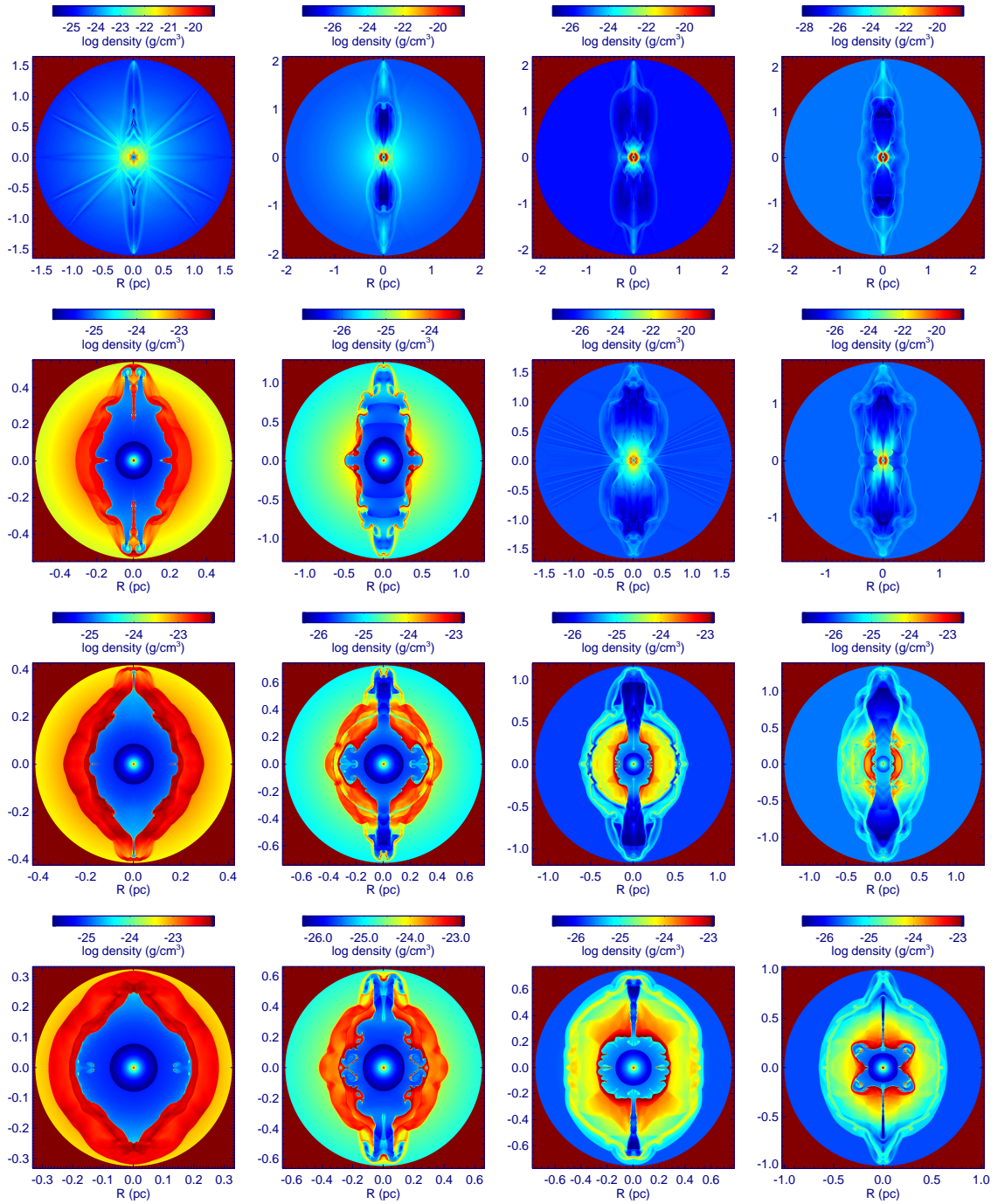


**Figure 5.** Logarithm of density for PN models B, C, E, F (top to bottom), with logarithm of AGB mass-loss rates in  $M_{\odot} \text{ yr}^{-1}$  of  $-6$ ,  $-7$ ,  $-8$ ,  $-9$  (from left to right) and a  $1.0 M_{\odot}$  (ZAMS) central star, at  $10,000$  yr of the evolution. The order is the same as in Table 1.

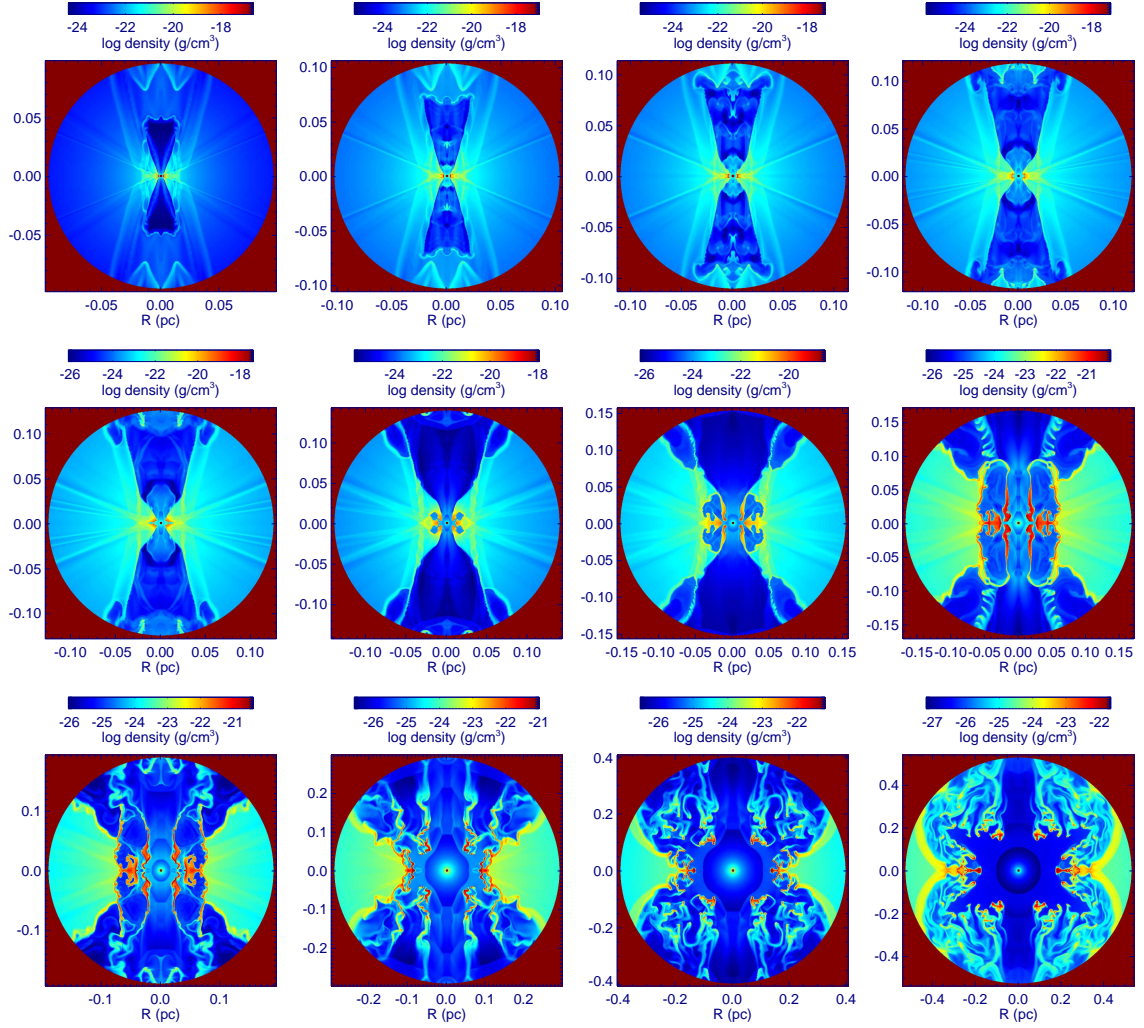


**Figure 6.** Logarithm of density at different snapshots (300, 400, 500, 600, 700, 900, 1,100, 1,300, 1,500, 2,000, 2,500 and 3,000 yr) of the central parts of Model C7-2.5, showing the fragmentation of the equatorial region. The last frame is also displayed in Figure 2.

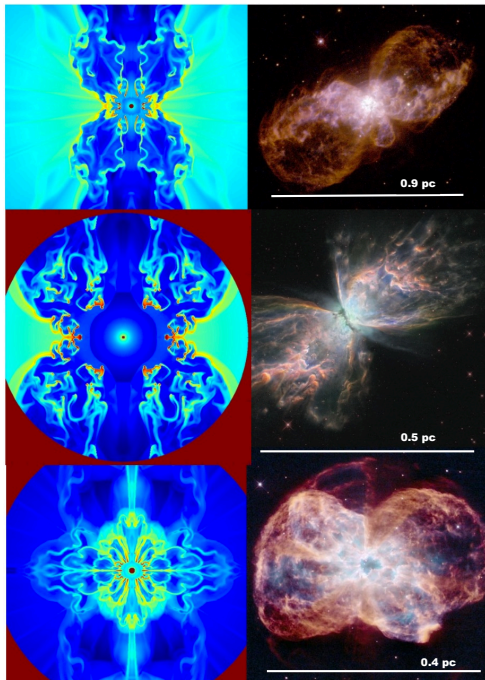


**Figure 7.** Examples of fragmentation and clumps. Left: density enlargement of models B6-2.5 (2,500 yr), C7-2.5 (2,500 yr) and C8-2.5 (3,000 yr). Right: Hubble 5, NGC 6302 and NGC 2440. Credit: NASA/ESA Hubble Space Telescope.

ever, a substantial amount of matter may return to within the binary orbit, which may facilitate merging of the system (Kuruwita et al. 2016). The properties of the binary system at the onset of the CE phase that we envision (yet to be determined) are such as to be bracketed by the systems leading to the above outcomes.

The models produce in general terms the typical morphologies observed in PNe, where most of the nebulae are elliptical (40.2%), followed by the bipolar class (22%) according to González-Santamaría et al. (2021). Our computations offer a new perspective for understanding the formation of elliptical nebulae that has not been previously discussed in the context of CEE, whereas bipolar nebulae have been attributed to binary interaction since the early work of Soker (1998).

The computations presented in this study show that bipolar nebulae can result from both low-mass and intermediate-mass progenitors. This result implies that, according to the observed abundances, bipolar PNe could be classified as type I or type II Peimbert (Peimbert 1978). However, there is a difference in the resultant morphology that could provide an indication of the progenitor mass. The difference resides in the type of lobes produced. In particular, central stars with larger masses have energetic winds at early phases, while low-mass progenitors do not present important winds at the same stage. This implies that larger masses will produce more rounded lobes (Figure 2 and 3), while lower masses will pro-

duce more elongated and sharp-pointed shapes similar to the PPN phase (Figure 4 and 5). The presence or absence (respectively) of diffuse X-rays also follows. Since soft X-rays are emitted by the hot shocked gas produced by the reverse shock of the fast, line-driven stellar wind, their detection indicates the existence of the fast wind (Kastner et al. 2000, Chu et al. 2001).

In addition, there is a difference in the resultant morphology that could provide a hint of the progenitor mass. The difference stems from the fragmentation of the nebula, the origin of which resides in the temporal evolution of the wind. Low-mass progenitors ( $1 M_{\odot}$ ) evolve very slowly towards the blue on the HR diagram, and their respective winds start to be dynamically important only at very late times (10,000 yr). On the other hand, the ionizing radiation is important earlier in time. This dictates that the dynamics of the nebula are almost totally governed by the expansion of the H II region, and the fragmentation is only based in the ionization-shock (I-S) front instability (García-Segura & Franco 1996). The I-S front instability occurs in D-type ionization fronts (Kahn 1954) and has a similar behavior as the thin-shell instability (Vishniac 1983). The thermal pressure in the thin-shell instability is provided by the hot shocked gas from a wind-blown bubble or a supernova remnant, while the thermal pressure in the I-S front instability is provided by the H II region.

This type of fragmentation produces cometary clumps aligned with the radiation field in the radial direction (Models E-1.0 and F-1.0 in Figure 4). These cometary clumps have been observed in a large number of PNe, for example in the Necklace nebula (Corradi et al. 2011) and NGC 2392 (Guerrero et al. 2021).

In contrast, more massive progenitors ( $2.5 M_{\odot}$ ) produce hot shocked gas from the fast line-driven winds at early phases. The shocked wind, in combination with the radiation field, can fragment the nebula in a different form, as shown in Figure 6. Here, the ionization front is very efficient in carving the neutral gas. The breaks made by the ionization front enable the hot gas to fill into these regions. However, the hot shocked gas can expand in the latitudinal direction very efficiently, and the resulting fragmentation does not only occur in the radial direction. Thus, multiple clumps are formed, with the difference that the tails of the clumps are not necessarily aligned in the radial direction. Figure 7 shows a comparison of three models with the nebulae Hubble 5, NGC 6302, and NGC 2440. The three nebulae display multiple clumps within the lobes that are reproduced in the models B6-2.5, C7-2.5, and C8-2.5. Furthermore, model C8-2.5 produces an outflow in the equatorial region not aligned with the major symmetry axis, produced by the focusing of hot shocked gas through the clumps. This may be similar to that observed in NGC 2440 (López et al. 1998). However, this effect could be an artifact of the 2-dimensional computation, since the clumps here are indeed rings from the imposed symmetry, and individual clumps could have a different behavior.

As a secondary goal of this paper, we checked whether or not the magnetically collimated outflows and jets computed in the PPN phase (Paper III) were long-lived structures. Our computations show that those structures disappear as soon as the line-driven wind is able to sweep up the collimated gas, leaving some remnants of them in only a few cases.

Based on either observational work (Sahai & Trauger 1998, Tafuya et al. 2020) or theoretical studies (Nordhaus & Black-

man 2006, Paper III, Blackman 2022) jets have been suggested to form at the early stages of PPNe. Based on the results of our simulations, we suggest that the observed jets in PNe (Guerrero et al. 2020) must be remnants of those early phases and are not being actively collimated during the PN phases (García-Segura 1997). This implies that “FLIERS” and “ansae” (Balick et al. 1993, Gonçalves et al. 2001) could be remnants of those jets.

Figures 2, 3, 4 and 5 show that PNe that form from PPNe with large sizes (for example models B7, B8 and B9) contain dense and compact cores. Note that the typical sizes of PPNe are of the order of 0.01 pc (Sahai & Trauger 1998), while here the sizes are  $\sim 0.2$  pc. The presence of these small cores results from the lower expansion velocity of the CEE ejecta and the slow x-wind (see Paper III). This effect produces dense gas close to the center of the nebula (most likely unresolved in some cases). These compact cores can provide an explanation for the very bright center in nebulae like the Red Spider Nebula (NGC 6537), as in model B8-2.5 (Figure 2). We note that the bright cores could be confused with the total sizes of PNe that are very distant and have low surface brightness. These models could possibly be related to the PN morphological class “compact or stellar type” and those unclassified nebulae that are unresolved in surveys (Schwarz et al. 1992, Corradi & Schwarz 1995, Machado et al. 1996).

## 5 CONCLUSIONS

It has been found that models for PNe evolving from magnetically driven PPNe that have undergone a CEE event are able to explain the majority of PN shapes, i.e., the elliptical and bipolar morphological classes. The point-symmetric class is not addressed in this paper, as such nebulae cannot be studied in the two-dimensional approximation. Three-dimensional axis-free computations will be required to investigate this class.

One and 2.5  $M_{\odot}$  (ZAMS) progenitors can form bipolar PNe, but there are differences in the resultant nebulae. Specifically, larger masses produce more rounded lobes, while lower masses produce more elongated and sharp-pointed shapes similar to the preceding PPN phase.

There is also a large difference in the fragmentation of PNe as a consequence of the central stellar mass. The fragmentation of low-mass PN progenitors produces cometary clumps aligned with the radiation field in the radial direction, mainly in the equatorial region producing “necklace”-type nebulae. On the other hand, larger masses give rise to the formation of multiple clumps in the latitudinal direction, which remain inside of the lobes, close to the center, are immersed in and surrounded by hot shocked gas, and are not necessarily aligned in the radial direction. Although the large difference in the fragmentation is mainly due to the progenitor mass, it is also an explicit fingerprint of a post-CE PPN. In particular, the fragmentation is made possible by the gas distribution in the previous post-CE PPN as shaped by the jets.

The magnetically collimated outflows and jets that are formed in the PPN phase disappear as soon as the line-driven wind is able to sweep up the collimated gas, leaving some remnants of their structure in the PN phase.

There are still many unknowns in the formation of planetary nebulae descended from CEE. For example, the relation-

ship between the mass ratios of the two stars and the ejection efficiency, the lifetime of the circumbinary disk, and the role of the accretion disk surrounding the secondary star remain to be studied. The formation of point-symmetric nebulae still remains challenging. These open questions will be part of our future work.

## ACKNOWLEDGEMENTS

We thank our referee, Orsola De Marco, for a careful reading of the manuscript and for her suggestions, which improved considerably the article. We thank Michael L. Norman and the Laboratory for Computational Astrophysics for the use of ZEUS-3D. The computations were performed at the Instituto de Astronomía-UNAM at Ensenada. G.G.-S. is partially supported by CONACyT grant 178253. Partial support for this work has been provided by NSF through grants AST-0200876 and AST-0703950.

## DATA AVAILABILITY

The data underlying this article will be shared on reasonable request to the corresponding author.

## REFERENCES

- Balick, B., Rugers, M., Terzian, Y., & Chengalur, J. N., 1993, *ApJ*, 411, 778
- Bujarrabal, V., Castro-Carrizo, A., Alcolea, J., & Sánchez-Contreras, C. 2001, *A&A*, 377, 868
- Blackman, Eric G., 2022, arXiv:2202.07246
- Clarke, D. A. 1996, *ApJ*, 457, 291
- Corradi, R. L. M., Sabin, L., Miszalski, B. et al, 2011, *MNRAS*, 410, 1349
- Corradi, R. L. M.; Schwarz, H. E, 1995, *A&A*, 293, 871
- Chu, Y.-H., Guerrero, M. A., Gruendl, R. A. et al., 2001, *ApJL*, 553, 69
- De Marco, O., 2009, *PASP*, 121, 316
- De Marco, O, et al., 2022, in preparation
- Frank, A., Chen, Z., Reichardt, T. et al., 2018, *Galax*, 6, 113
- Frank, A. & Mellema, G. 1994, *A&A*, 289, 937
- García-Segura, G. 1997, *ApJ*, 489, 189
- García-Segura, G., & Franco, J., 1996, *ApJ*, 469, 171
- García-Segura, G., Langer, N., Różyńska, M., & Franco, J. 1999, *ApJ*, 517, 767
- García-Segura, G., López, J. A., Steffen, W., Meaburn, J. and Machado, A. 2006, *ApJL*, 646, L61
- García-Segura, G., Ricker, P. M., & Taam, R. E., 2018, *ApJ*, 860, 19, paper I
- García-Segura, G., Taam, R. E., & Ricker, P. M., 2020, *ApJ*, 893, 150, paper II
- García-Segura, G., Taam, R. E., & Ricker, P. M., 2020, *ApJ*, 914, 111, paper III
- Gonçalves, D. R., Corradi, R. L. M.; Mampaso, A., 2001, *ApJ*, 547, 302
- González-Bolívar, M., De Marco, O., Lau, M. Y. M., Hirai, R., & Price, D. J., 2022, *MNRAS*, in press, arXiv:2205.09749
- González-Santamaría, I., Manteiga, M., Machado, A. et al., 2021, *A&A*, 656, 51
- Guerrero, M. A., Cazzoli, S., Rechy-García, J. S. et al, 2021, *ApJ*, 909, 44
- Guerrero, M. A., Rechy-García, J. S., & Ortiz, R., 2020, *ApJ*, 890, 50

- Icke, V., Preston, H. L. & Balick, B. 1989, *AJ*, 97, 462
- Ivanova, N., Justham, S., Chen, X. et al. 2013, *A&ARv*, 21, 59
- Kahn, F. D., 1954, *BAN*, 12, 187
- Kastner, J. H., Soker, N., Vrtilik, S. D., & Dgani, R., 2000, *ApJL*, 545, 57
- Jones, D., & Boffin, H. M. J., 2017, *NatAs*, 1, 117
- Kuruwita, R. L., Staff, J., & De Marco, O., 2016, *MNRAS*, 461, 486
- Kwitter, K. B., & Henry, R. B. C., 2022, *PASP*, 134, 2001
- López, J. A., Meaburn, J., Bryce, M., & Holloway, A. J. , 1998, *ApJ*, 493, 803
- MacDonald, J. & Bailey, M. E. 1981, *MNRAS*, 197, 995
- Manchado, A., Guerrero, M., Stanghellini, L., & Serra-Ricart, M., 1996, “The IAC Morphological Catalog of Northern Galactic Planetary Nebulae”, ed. Instituto de Astrofísica de
- Mellema, G., 1993, Ph. D. thesis, University of Leiden
- Mellema, G., Eulderink, F. & Icke, V. 1991, *A&A*, 252, 718
- Miszalski, B., Acker, A., Parker, Q. A., & Moffat, A. F. J. 2009, *A&A*, 505, 249
- Nordhaus, J., & Blackman, E. G., 2006, *MNRAS*, 370, 2004
- Ondratschek, P. A., R., Friedrich K., Schneider, F. R. N. et al., 2022, *A&A*, 660, 8
- Paczyński, B., 1971, *ARA&A*, 9, 183
- Peimbert, M., 1978, *IAU Symp. No 76*, “Planetary Nebulae: Observations and Theory”, ed. Y. Terzian (D. Reidel Publishing Company, Dordrecht), 215
- Raymond, J. C. & Smith, B. W. 1977, *ApJS*, 35, 419
- Ricker, P. M., & Taam, R. E. 2012, *ApJ*, 746, 74
- Sahai, R., & Trauger, J. T., 1998, *AJ*, 116, 1357
- Soker, N., 1997, *ApJS*, 112, 487
- Soker, N. 1998, *ApJ*, 496, 833
- Schwarz, H. E., Corradi, R. L. M. & Melnick, J., 1992, *A&A Suppl.*, 96, 23
- Stone, J. M. & Norman, M. L. 1992, *ApJS*, 80, 753
- Taam, R. E., Bodenheimer, P., & Ostriker, J.P., 1978, *ApJ*, 222, 269
- Tafoya, D., Imai, H., Gomez, J. F. et al., 2020, *ApJ*, 890, 14
- Vassiliadis, E., & Wood, P. 1994, *ApJS*, 92, 125
- Villaver, E., Manchado, A., & García-Segura, 2002, *ApJ*, 581, 1204
- Vishniac, E. T., 1983, *ApJ*, 274, 152
- Zou, Y., Frank, A., Chen, Z. et al., 2020, *MNRAS*, 497, 2855

This paper has been typeset from a  $\text{\TeX}/\text{\LaTeX}$  file prepared by the author.